Biomaterials Science

ROYAL SOCIETY OF CHEMISTRY

PAPER

View Article Online
View Journal | View Issue

Cite this: *Biomater. Sci.*, 2023, **11**, 2860

Phenotypic and transcriptional characterization of oligodendrocyte precursor cells in a 3D culture

Shizuka Nakano,[a,b,c] Akiko Uyeda,[a] Yukiko T. Matsunaga *[b,c] and Rieko Muramatsu*[a]

Remyelination of the central nervous system (CNS) is a regenerative response that depends on the development of oligodendrocyte precursor cells (OPCs), which are generated from neural stem cells in developmental stages and exist as tissue stem cells in the adult CNS. Three-dimensional (3D) culture systems that recapitulate the complexity of the *in vivo* microenvironment are important for understanding the behavior of OPCs in remyelination and for exploring effective therapeutic approaches. In general, functional analysis of OPCs has mainly used two-dimensional (2D) culture systems; however, the differences between the properties of OPCs cultured in 2D and 3D have not been fully elucidated despite cellular functions being affected by the scaffold. In this study, we analyzed the phenotypic and transcriptomic differences in OPCs from 2D and collagen gel-based 3D cultures. In the 3D culture, the OPCs exhibited less than half ratio of proliferation and almost half ratio of differentiation to mature oligodendrocytes, compared to the 2D culture in the same culturing period. RNA-seq data showed robust changes in the expression level of genes associated with oligodendrocyte differentiation, and there were more up-regulated genes than down-regulated genes in 3D cultures compared to 2D cultures. In addition, the OPCs cultured in collagen gel scaffolds at lower collagen fiber densities showed higher proliferation activity compared with those cultured in collagen gel with higher collagen fiber densities. Our findings have identified the effect of culture dimension as well as the complexity of the scaffold on OPC responses at the cellular and molecular levels.

Received 18th November 2022,
Accepted 12th February 2023

DOI: 10.1039/d2bm01897g

rsc.li/biomaterials-science

1. Introduction

Demyelination is a particular feature of pathological lesions in central nervous system (CNS) diseases, such as multiple sclerosis, Alzheimer's disease, amyotrophic lateral sclerosis, and many other neurological and psychiatric disorders.[1–3] CNS myelin is formed by oligodendrocytes, a kind of glial cell.[4] Demyelination is characterized by loss of the myelin sheath and oligodendrocyte cell death resulting in severe neurological deficits.[5] However, neurological deficits often partially resolve spontaneously, which is thought to be dependent on myelin repair and remyelination around the lesion.[6] In addition to developmental myelination, remyelination in response to CNS damage is considered to be initiated by the proliferation of oligodendrocyte precursor cells (OPCs), tissue stem cells that are distributed throughout the CNS in adult mammals, followed by differentiation into mature oligodendrocytes that achieve axon wrapping.[7] A better understanding of oligodendrocyte properties is of interest in terms of developing treatments for CNS demyelinating diseases with a well-established etiology due to demyelination.

The mechanisms underlying oligodendrocyte development, including OPC proliferation and differentiation into mature oligodendrocytes, have been examined in cultured OPCs, which are either primary cells or derived from stem cells.[8,9] Most experiments have used two-dimensional (2D) culture systems because they are highly reproducible and scalable. However, 2D cultures generally lack sufficient cell–cell interaction and cytoarchitecture *in vitro*; therefore, 2D cultures are limited in that they cannot mimic the cellular response in a three-dimensional (3D) environment such as *in vivo*.[10] Consequently, recent studies have shown that OPCs can change their phenotypes, such as survival, migration, and proliferation, in response to a variety of cues from the microenvironment: not only to chemical cues from other cells, but also to physical and mechanical cues such as stiffness, strain, and

[a]*Department of Molecular Pharmacology, National Institute of Neuroscience, National Center of Neurology and Psychiatry, 4-1-1 Ogawa-higashi, Kodaira, Tokyo 187-8502, Japan. E-mail: muramatsu@ncnp.go.jp; Fax: +81-42-346-1755; Tel: +81-42-346-1725*
[b]*Institute of Industrial Science, The University of Tokyo, 4-6-1 Komaba, Meguro-ku, Tokyo 153-8505, Japan. E-mail: mat@iis.u-tokyo.ac.jp; Fax: +81-3-5452-6471; Tel: +81-3-5452–6470*
[c]*Department of Bioengineering, School of Engineering, The University of Tokyo, 7-3-1 Hongo, Bunkyo-ku, Tokyo 113-8656, Japan*

topography of the extracellular matrix (ECM).[11–13] Considering that the physical and mechanical landscape of a CNS changes during development, aging, and pathological conditions, 3D cultures are a powerful tool in establishing microphysiological system (MPS) platforms to evaluate cell responses because 3D culture systems can recapitulate more complex cell–cell or cell–ECM interactions than 2D systems, thereby more closely resembling *in vivo* microenvironments. 3D culture studies can be conducted either by creating the cultured tissue itself in 3D (*e.g.*, organoid, spheroid) or by creating the environment surrounding the cell in 3D (using ECM components), offering tractable models of human CNS diseases.[14–16] The latter is suitable for analyzing the effects of the extracellular environment on the cell. Collagen, classified as a hydrogel, has been the most commonly used ECM scaffold in 3D cultures of CNS cells including OPCs,[17,18] because it demonstrates the contractile nature of the cells.[19] Collagen, in terms of nervous system repair, presents many advantages, such as being remarkably biocompatible, biodegradable, versatile, and nontoxic. Therefore, collagen is widely used in Food and Drug Administration (FDA)-approved nerve conduits and nerve cuffs for peripheral nerve repair and has received much attention for its potential use in the treatment of brain diseases. Although a number of approaches have been developed to culture CNS cells in 3D culture systems which mimic the CNS microenvironment using various ECMs containing laminin and hyaluronic acid,[20,21] the phenotypic and transcriptomic differences in OPCs between 2D and 3D cultures remain unknown.

In this study, we compared the properties of OPCs from 2D and collagen gel-based 3D cultures. We used mouse primary OPCs and evaluated OPC proliferation and differentiation between 2D and 3D cultures. We also conducted RNA-seq analysis and found robust differences in the expression of genes involved in oligodendrocyte differentiation and myelination between OPCs cultured in 2D and 3D.

2. Materials and methods

2.1. Primary culture of oligodendrocytes

Postnatal day 1 (P1) C57BL/6J mice were obtained from Tokyo Laboratory Animals Science. All animal procedures were performed in accordance with the Guidelines for Care and Use of Laboratory Animals of the National Institutes of Neuroscience, National Center of Neurology and Psychiatry (NCNP) and approved by the Animal Ethics Committee of the NCNP (2021013R2).

Primary OPC cultures were obtained from the mice at P1, as previously described.[22] The mouse forebrains were dissected and minced in ice-cold phosphate-buffered saline (PBS) using fine scissors. The minced tissues were dissociated with 0.125% trypsin (15090-046, Thermo Fisher Scientific, Waltham, MA, USA) in PBS at 37 °C for 10 min. After neutralization with Dulbecco's modified Eagle's medium (DMEM; 12800082, Thermo Fisher Scientific) containing 10% fetal bovine serum (FBS; F7524; Sigma-Aldrich, St. Louis, MO, USA), the cells were centrifuged at 400*g* for 10 min, suspended in 10% FBS-DMEM, and filtered through a 70 μm-pore nylon cell strainer. The cells were then plated onto a poly-L-lysine (PLL; P2636, Sigma)-coated 10 cm dish and cultured in 10% FBS-DMEM supplemented with penicillin–streptomycin (PS; 164-25251, Fuji Film Wako, Osaka, Japan) at 37 °C with 5% CO_2. Eleven days after culturing, the cells were rinsed with PBS, and the remaining cells were treated with 0.05% trypsin-PBS at 37 °C for 3 min. After neutralization with 10% FBS-DMEM, the detached cells were filtered through a 40 μm-pore nylon cell strainer and collected by centrifugation at 400*g* for 5 min. The collected cells were then replated onto a non-coated 10 cm dish and cultured for 30 min at 37 °C with 5% CO_2. The non-adherent cells (OPCs) were collected for use in the experiments (about 60% of cells in the culture were co-labeled with Olig2[22]).

Isolated OPCs were then separated into two groups and either cultured on glass (2D culture) or in a type I collagen matrix (3D culture). For the 2D culture, the OPCs were suspended at 5×10^5 cells per mL in an OPC medium composed of DMEM supplemented with 4 mM L-glutamine (Sigma-Aldrich), 1 mM sodium pyruvate (S8636, Sigma-Aldrich), 1% PS, 0.1% bovine serum albumin (BSA; Sigma-Aldrich), 50 μg mL^{-1} apo-transferrin (T5391, Sigma-Aldrich), 5 μg mL^{-1} insulin (I1882, Sigma-Aldrich), 30 nM sodium selenite (S9133, Sigma-Aldrich), 10 nM biotin (B4639, Sigma-Aldrich), 10 nM hydrocortisone (H0888, Sigma-Aldrich), 10 ng mL^{-1} platelet-derived growth factor-AA (PDGF-AA; 315-17, PeproTech), and 10 ng mL^{-1} basic fibroblast growth factor (b-FGF; 450-33, PeproTech). The OPC suspension was applied to a PLL-coated 96-well glass bottom plate (5866-096, IWAKI, Shizuoka, Japan) at a density of 5×10^4 cells per well. For the 3D culture, the OPCs were suspended at 2×10^6 cells per mL in a neutralized type I collagen solution. The collagen solution was prepared by mixing a Cellmatrix Type I-A collagen solution (3 mg mL^{-1}, Nitta Gelatin, Osaka, Japan) with 10× Hanks' buffer (H1641, Sigma-Aldrich) and 10× collagen buffer (262 mM $NaHCO_3$ and 20 mM HEPES in 0.05 N NaOH) at a volume ratio of 8 : 1 : 1 (final collagen concentration of 2.4 mg mL^{-1}). For the study with lower collagen gel concentrations (final concentration, 0.6 mg ml^{-1}), the Cellmatrix Type I-A collagen solution (3 mg ml^{-1}) was diluted at 0.75 mg mL^{-1} with HCl (pH = 3) and then neutralized in the same manner. The OPCs suspended in the neutralized collagen solution (2.4 mg ml^{-1}, 25 μl per well) were placed on a non-coated 96-well glass bottom plate at a density of 5×10^4 cells per well. The plates were centrifuged at 216*g* for 1 min to homogeneously spread the collagen solution and incubated for 10 min at 37 °C with 5% CO_2. After gelation of the collagen solution, the OPC medium was added to each well. The cells in 2D and 3D culture systems were maintained at 37 °C with 5% CO_2 for 3 days to assess the responsiveness of OPCs to stimuli.[11,12,23,24] Cell aggregation was not observed with this centrifugation process.

Three days after culturing, the cells were treated with a differentiation medium composed of DMEM supplemented with 4 mM L-glutamine, 1 mM sodium pyruvate, 0.1% BSA,

50 μg mL^{-1} apo-transferrin, 5 μg mL^{-1} insulin, 30 nM sodium selenite, 10 nM biotin, 10 nM hydrocortisone, 1% penicillin–streptomycin, and 40 ng mL^{-1} 3,3′,5-triiodo-L-thyronine sodium salt (T3; T2752, Sigma-Aldrich).

2.2. Immunocytochemistry

The cells were fixed with 4% paraformaldehyde (PFA; 104005, Merck, Darmstadt, Germany) in PBS at room temperature (RT) for 30 min and permeabilized and blocked with a blocking solution, which was composed of 3% normal donkey serum (NDS; IHR-8135, IBC, Mukilteo, WA, USA) and 0.5% Triton X-100 (12967-45, Nacalai Tesque, Kyoto, Japan), in PBS for 30 min at RT. The cells were then incubated in the blocking solution overnight at 4 °C with primary antibodies diluted at 1 : 800 (2D) and 1 : 600 (3D). The following antibodies were used: rat anti-Ki67 antibody (14-5698-82, Invitrogen, Waltham, MA, USA), rabbit anti-cleaved caspase-3 antibody (CC3; 9661S, Cell Signaling Technology, Danvers, MA, USA), mouse anti-Olig2 antibody (MABN50, MERCK), and goat anti-Olig2 antibody (AF2418, Bio-Techne, Minneapolis, MN, USA). The samples were then incubated for 4 h at RT with a blocking buffer containing secondary antibodies diluted at 1 : 800 (2D) and 1 : 600 (3D). The following antibodies were used: Alexa Fluor 488-conjugated donkey antibody agonist, mouse IgG; Alexa Fluor 594-conjugated donkey antibody agonist, rat IgG; and Alexa Fluor 647-conjugated donkey antibody agonist, rabbit or goat IgG (Thermo Fisher Scientific). The nuclei were subsequently stained with 4′,6-diamidino-2-phenylindole (DAPI, 1 : 5000) for 10 min. To stain the collagen fibers, the samples were incubated with the conjugate of mouse monoclonal anti-collagen I antibody (ab6308, Abcam, Cambridge, UK) and Alexa Fluor 488-conjugated donkey antibody agonist mouse IgG diluted at 1 : 100 in blocking solution overnight at RT.

Fluorescence images were captured using a confocal laser scanning microscope (FV3000; Olympus, Tokyo, Japan) with a 20×/0.80 objective lens at four different locations in each sample. At each location, a 100 μm stack with 5 μm thick slices from the bottom glass plate was obtained, resulting in a total image size of 636 μm × 636 μm and 1024 × 1024 pixels in each 2D image. The percentage of Ki67-positive or CC3-positive Olig2-positive cells was quantified using image processing software Fiji (ver 2.1.0/1.53c).[25] To characterize the collagen fiber density in the 3D culture, the collagen fiber intensity was quantified by measuring the mean intensity of the obtained confocal images (single plane: 636 μm × 636 μm, 1024 × 1024 pixels, 5 μm thick, total thickness: 100 μm) using Fiji. A heat map of the collagen fiber intensity was generated from the single plane images by dividing them into 40 μm × 40 μm squares with 64 × 64 pixels. The collagen fiber density around the Ki67 positive/negative and Olig2 positive cells was measured using the mean intensity of the maximum intensity projection image (single plane: 62 μm × 62 μm, 100 × 100 pixels, 5 μm thick, total thickness: 20 μm). The histogram of the collagen fiber intensity around the Ki67 positive/negative and Olig2 positive cells is expressed as the mean cell number percentage in each experiment for each collagen fiber intensity.

2.3. Quantitative reverse transcription polymerase chain reaction (RT-PCR) and RNA-seq analysis

Total RNA was collected from the OPCs using an RNeasy Micro Kit (74004, Qiagen, Hilden, Germany). For quantitative RT-PCR, cDNA was synthesized using an RT-RamDA cDNA Synthesis Kit (Toyobo, Osaka, Japan) and real-time RT-PCR was performed using a KOD SYBR qPCR Mix (QKD-201, Toyobo) with the following primer pairs: *mbp* forward, GGCGGTGACAGACTCCAAG; *mbp* reverse, GAAGCTCG-CGGACTCTGAG; *gapdh* forward, TCACCACCATGGAGAAGGC; *gapdh* reverse, GCTAAGCAGTTGGTGGTGCA. PCR conditions included one cycle at 98 °C for 120 s, followed by 39 cycles at 98 °C for 10 s, 60 °C for 10 s, and 68 °C for 30 s. Melting analysis was performed using PCR to monitor amplification specificity. Relative mRNA expression was normalized to *gapdh* mRNA levels in the same samples and calculated using the Δ/Δ-Ct method.

For the RNA-seq analysis, the total RNA of the OPCs was collected three days after culturing in the OPC medium. Library preparation was performed using a TruSeq stranded mRNA sample prep kit (Illumina), according to the manufacturer's instructions. Whole-transcriptome sequencing was performed on the RNA samples using an Illumina HiSeq 2500 platform in 75-base single-end mode. Base calling was performed using Illumina Casava ver.1.8.2 software. Sequenced reads were mapped to mouse reference genome sequences (mm10) using TopHat ver. 2.0.13, in combination with Bowtie2 ver. 2.2.3 and SAMtools ver. 0.1.19. The number of fragments per kilobase of exons per million mapped fragments (FPKMs) was calculated using Cufflinks ver. 2.2.1. The RNA-seq data presented were from replicate 3, and all trends were observed in both replicates. Differentially expressed genes were defined as a fold change > 2.0 and a q-value < 0.1. Gene ontology analysis was performed using the Database for Annotation, Visualization, and Integrated Discovery v6.8.[26,27]

2.4. Statistical analysis

Data are presented as the mean ± standard error of the mean (SEM). Statistical significance between groups was determined using the unpaired Student's t-test or the Kolmogorov–Smirnov test. All data were analyzed using Excel 2019 (Microsoft), R, or MATLAB.

3. Results

3.1. OPCs in collagen gel displayed reduced cell proliferation and maturation

To investigate the phenotypic differences between 2D and 3D cultures from the viewpoints of viability, proliferation, and differentiation during maturation, we cultured mouse primary OPCs on glasses (2D) or in collagen gels (3D). We first assessed the viability of the OPCs by immunocytochemical analysis of

cleaved caspase 3 (CC3), an apoptotic marker (Fig. 1A). Similar to the 2D culture, the 3D culture showed a low ratio of number of $CC3^+$ $Olig2^+$ cells to the total number of $Olig2^+$ cells (day 1: 0.3 ± 0.1% (2D), 1.6 ± 0.5% (3D); day 2: 0.3 ± 0.1% (2D), 1.7 ± 0.3% (3D); day 3: 0.2 ± 0.0% (2D), 2.0 ± 1.3% (3D)), and there were no significant differences between 2D and 3D cultures at any culturing day (Fig. 1A and B), indicating that a 3D culture under the conditions of our study is able to maintain OPC survival as well as a 2D culture. The $Olig2^+$ cell density in the 2D culture was decreased throughout the experiment (day 1: 357.9 ± 72.1; day 2: 206.1 ± 16.8; day 3: 160.9 ± 7.6), while that in 3D was retained (day 1: 122.6 ± 18.7; day 2: 129.6 ± 21.3; day 3: 90.1 ± 17.4), suggesting that remaining of apoptotic cells in the 3D culture gel, while releasing of them from the 2D culture surface, resulted in a relatively high ratio of apoptotic cells in the 3D culture compared to the 2D culture. To investigate the response of OPCs proliferating in 2D and 3D cultures, we detected the expression of Ki67, a proliferation marker (Fig. 1C). Immunocytochemical analysis showed that the ratio of $Ki67^+$ $Olig2^+$ cells to the total $Olig2^+$ cells in the 2D culture was 22.7 ± 3.6% after three days of culturing, similar to a previous report.[28] In contrast, OPCs in the 3D culture exhibited a

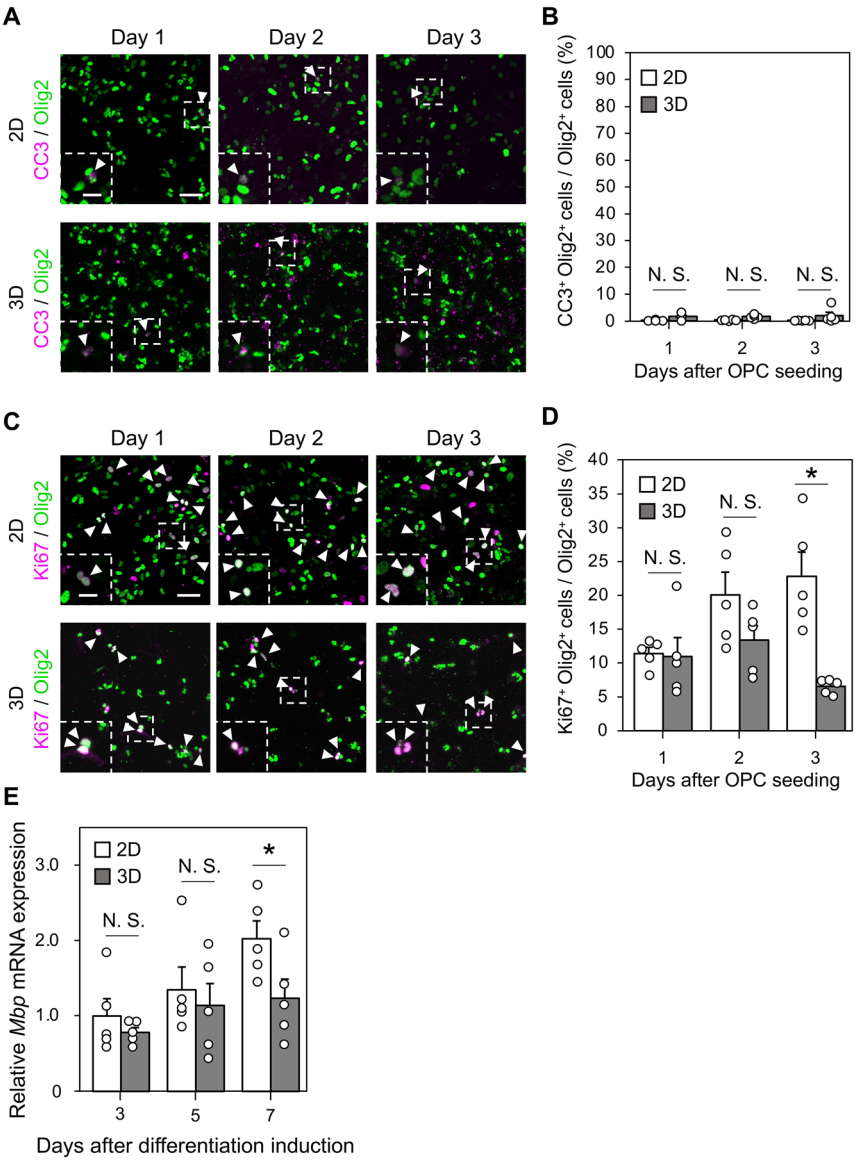

Fig. 1 3D culture reduces OPC proliferation and differentiation compared to 2D culture. (A) Representative images of the OPC cultures in 2D and 3D (collagen concentration, 2.4 mg mL^{-1}) stained with cleaved-caspase 3 (CC3; magenta) and Olig2 (green). The dashed square areas show the high magnification images of CC3 and Olig2 positive cells. (B) Quantification of the percentage of CC3 and Olig2-positive cells (arrowheads in A) in Olig2-positive cells. (C) Representative images of the OPCs cultured in 2D and 3D stained with Ki67 (magenta) and Olig2 (green). The dashed square areas show the high magnification images of Ki67 and Olig2 positive cells. (D) Quantification of the percentage of Ki67 and Olig2-positive cells (arrowheads in C) in Olig2-positive cells. (E) Quantification of the relative mRNA expression of *mbp* normalized by an internal control (*gapdh*). Error bars represent SEM. $N = 5$ for each, $*p < 0.05$. Scale bars represent 50 μm for low magnification and 20 μm for high magnification.

significantly lower ratio of $Ki67^+$ cells (6.5 ± 0.5% after three days of culturing) (Fig. 1D), suggesting that OPCs cultured in 3D have a milder proliferative capacity than those cultured in 2D.

To determine whether OPCs change their response during maturation depending on the culture dimension, we evaluated the ratios of oligodendrocyte differentiation in OPCs between the cultures. We induced OPC differentiation in a T3-containing medium, a well-established condition that sufficiently differentiates OPCs from mature oligodendrocytes in 2D cultures.[29] After culturing, we detected the mRNA of *myelin basic protein* (*mbp*) which is a differentiation marker for mature oligodendrocytes, in all samples. In both 2D and 3D cultures, the OPCs showed increased differentiation with passing culture time. However, the OPCs in the conventional 2D culture after 7 days of culturing showed a higher mRNA expression than those in the 3D culture (Fig. 1E). These data indicate that OPCs cultured in 3D retain their differentiation capacity, but with a low sensitivity against the induction of differentiation compared to that in the 2D culture.

3.2. OPCs in collagen gel decreased gene expression associated with OPC proliferation and maturation

Next, we performed an RNA-seq analysis to reveal the differences in the gene expression of OPCs in 2D or 3D cultures when treated with an OPC proliferation medium for three days. A principal component analysis indicated that the gene expression profile of 3D-cultured OPCs clearly differed from that of 2D-cultured OPCs (Fig. 2A). We found that 329 genes were downregulated and 645 genes were upregulated in 3D-cultured OPCs compared with 2D-cultured OPCs (Fig. 2B). To examine the characteristics of the genes whose expression was altered by the 3D culture, we performed a gene ontology (GO) analysis of these differentially expressed genes (DEGs) (fold change > 2.0, FDR < 0.1). The DEGs in 3D were more enriched in terms of cell–matrix adhesion (GO:0007160) compared to those in 2D (Fig. 2C), indicating that the 3D microenvironment induces OPC functional changes at the transcriptional level. Our 3D culture used collagen, which binds to receptors expressed on the cell surface of OPCs, including integrin receptors.[30] We detected DEGs related to the integrin-mediated signalling pathway (GO:007229, Fig. 2D), supporting the idea that a collagen-based 3D culture also changes the gene expression in OPCs depending on the interaction strength with the microenvironment.

We next searched for DEGs related to our observation of the difference in OPC proliferation between 2D and 3D cultures. GO analysis revealed that DEGs were enriched in GO terms related to the regulation of cell proliferation (Fig. 3A). We detected low levels of *Nog* and *lrp2*, which were annotated with the positive regulation of oligodendrocyte progenitor proliferation (GO:00070447)[31,32] in the 3D culture (Fig. 3B), supporting our observation that the 3D culture showed a low ratio of OPC proliferation compared to the 2D culture.

OPC proliferation is the initial process of remyelination, but proliferated OPCs are required to differentiate into mature oligodendrocytes to successfully remyelinate. Therefore, we investigated whether 3D culture-dependent transcriptional changes in OPCs were involved in oligodendrocyte differentiation. We found differences in the expression of genes annotated with GO terms related to oligodendrocyte differentiation (Fig. 3C: *tlr2*, *tnfrsf1b*, *il33*, and *il34* were up-regulated, while *cxcr4* was down-regulated) and myelination (Fig. 3D: *egr2*, *tnfrsf1b*, and *trf* were up-regulated, while *myrf* and *s100b* were down-regulated). These results suggested that such an alteration of gene expression in the 3D culture resulted in low sensitivity to differentiation induction compared to that in the 2D culture (Fig. 1E).

3.3. Improved OPC proliferation in a low collagen concentration matrix

Finally, we assessed whether the phenotypic changes of the OPC culture in 3D are affected by the density of collagen fibers around the cells because 3D material properties such as stiffness and degradability affect the stemness of neural progenitor cells.[33] In a preliminary experiment, we prepared 0.4–2.4 mg mL^{-1} of collagen gel and confirmed that 0.6 mg mL^{-1} was the lowest concentration needed for polymerization (data not shown). Thus, we decided to compare the OPC functions in the collagen gel at 0.6 mg mL^{-1} (low concentration) and 2.4 mg mL^{-1} (high concentration). Immunocytochemical analysis revealed that OPC viability, which was measured by the ratio of the number of $CC3^+$ $Olig2^+$ cells to the total number of $Olig2^+$ cells, was not significantly different between the groups (Fig. 4A and B; low concentration, 1.0 ± 0.2%; high concentration, 0.8 ± 0.2%). However, OPC proliferation measured by the ratio of the number of $Ki67^+$ $Olig2^+$ cells to the total number of $Olig2^+$ cells was significantly higher in low concentration cultures than in high concentration cultures (Fig. 4C and D; low concentration, 7.4 ± 0.3; high concentration, 4.6 ± 0.4%). There were no significant differences in the *mbp* mRNA levels cultured in OPCs under induced differentiation into oligodendrocytes between the groups (Fig. 4E). These data suggest that increasing the microenvironmental complexity by increasing the concentration of collagen gel impairs OPC proliferation.

To explore the relationship between the collagen density and OPC proliferation in the arrangement of microscale fiber networks, we characterized the spatial distribution of collagen fibers in the gels. The fluorescent images of collagen fibers revealed a heterogeneous distribution of collagen fiber density in the low concentration of collagen gel (0.6 mg mL^{-1}) (Fig. 4F). We then measured the intensity of collagen signals around $Olig2^+$ cells (Fig. 4G) and compared the distribution of collagen intensity around the proliferating OPCs. Interestingly, quantitative analysis revealed that proliferative $Ki67^+$ $Olig2^+$ cells were more localized in areas with a lower collagen fiber density than non-proliferative $Ki67^-$ $Olig2^+$ cells (Fig. 4H–J). These data indicate that OPCs sense collagen fiber densities and change their proliferation phenomena, suggesting that OPC proliferation can be tuned by the spatial distribution of the collagen fiber density.

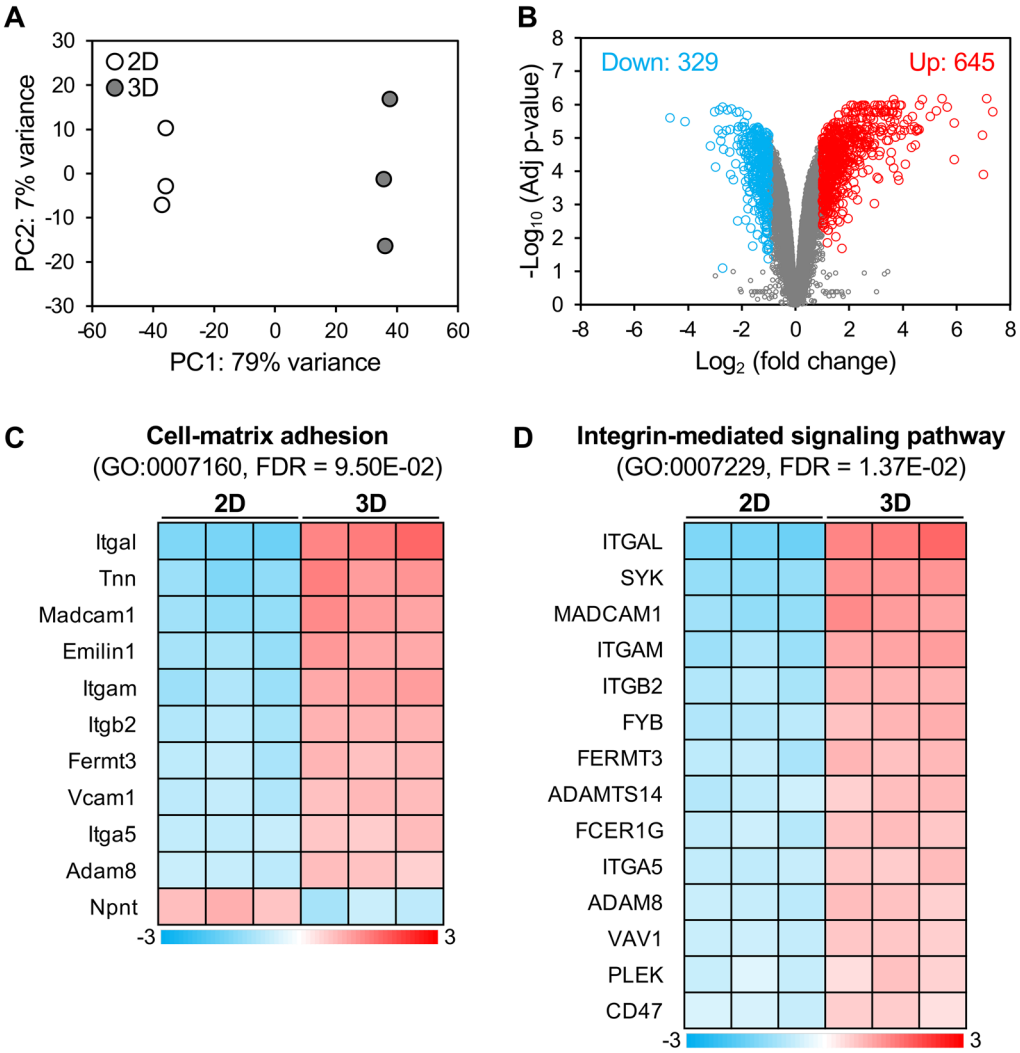

Fig. 2 3D culture changes the transcriptome profiles of OPCs. (A) Principal component analysis of RNA-seq data indicate the separation of gene expression in the OPCs cultured in 2D or 3D. PC, principal component. (B) Volcano plot of RNA-seq data from OPCs cultured in 2D or 3D. Differentially expressed genes (DEGs; fold change > 2, FDR < 0.1) are highlighted in blue (downregulated) or red (upregulated). (C and D) Summary of DEGs related to cell–matrix adhesion (C) and the integrin-mediated signaling pathway (D). Heat maps show mean-centered $\log_2$(FPKM + 1) on the color scale. Rows and columns represent genes and samples, respectively. *N* = 3 for each.

4. Discussion

In this study, we examined the phenotypic and gene expression changes in OPCs using 2D and 3D collagen gel cultures and found that OPCs have lower cell proliferation and differentiation abilities in 3D cultures than in 2D cultures. We also found that the phenotypic changes correlated with the changes in gene expression related to cell proliferation, differentiation, and myelin formation in OPCs. Furthermore, we found that the reduction in cell proliferation was dependent on the higher concentration of collagen encapsulated in the 3D culture.

OPCs cultured in our 3D culture system showed a reduction in the proliferation rate compared to the conventional 2D culture system, which was accompanied by robust changes in the transcriptional properties. Regarding the role of collagen type I, the principal component of the matrix used for the 3D culture, pathological deposition of the collagen type I-rich ECM is the hallmark of fibrosis, which is a common response to injury and inflammation and has also been found in CNS injuries.[34,35] Although OPCs have been known to be anchorage-dependent cells, and the interactions between the integrins expressed by OPCs and ECM proteins play a key role in the proliferation of OPCs,[30] collagen type I has been reported not to have an effect on the proliferation of OPCs when it was coated on the plate of under 2D culture conditions.[35] In contrast, we found a OPC proliferation acitivity was reduced in collagen-gel based 3D culture, suggesting that enriched interaction with collagen type I under 3D culture further alter downstream signaling.[36] Indeed, we found changes in the expression of integrins, including the subunit of receptors for collagen type I, such as *Itga2*, and downstream signaling mole-

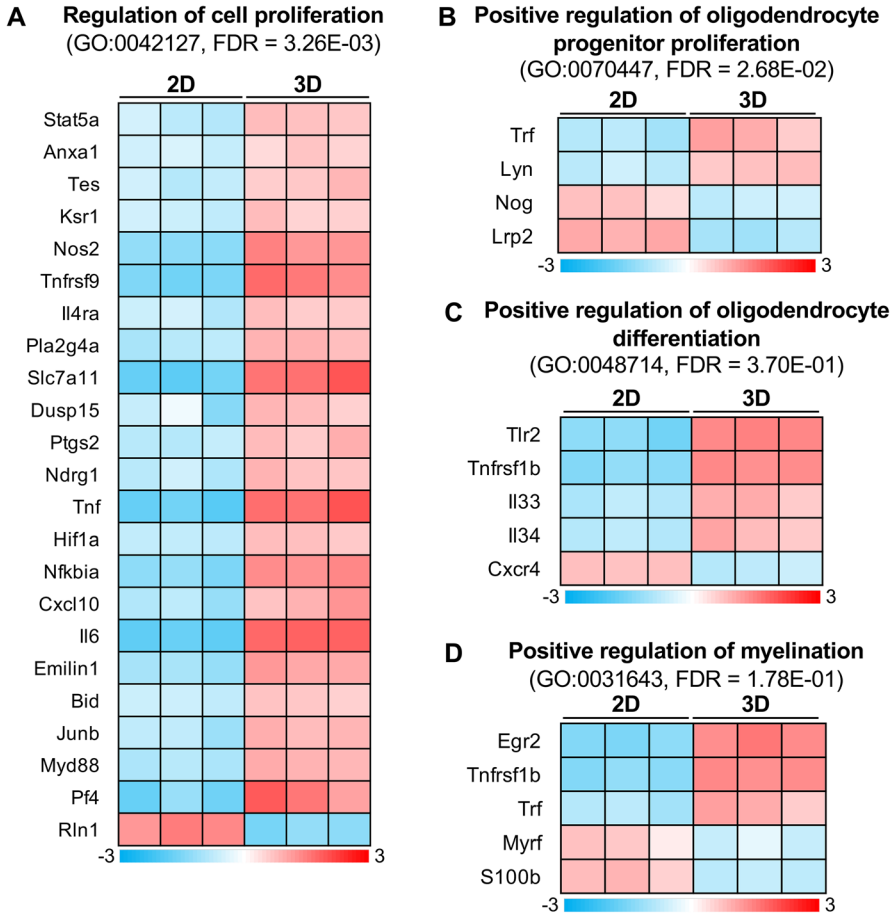

Fig. 3 3D culture causes expression changes in the genes of oligodendrocyte development. (A–D) Summary of DEGs related to the regulation of cell proliferation (A), positive regulation of oligodendrocyte progenitor proliferation (B), positive regulation of oligodendrocyte differentiation (C), and positive regulation of myelination (D). Heat maps show mean-centered $\log_2$(FPKM + 1) on the color scale. Rows and columns represent genes and samples, respectively.

cules, supporting the notion that changes in the interaction strength with the ECM affect the gene expression of OPCs, whereby the culture dimension regulates cell proliferation.

Regarding OPC differentiation into oligodendrocytes, we found that OPCs cultured in 3D showed a lower efficiency of OPC differentiation. OPC differentiation is experimentally induced using T3, the active form of the thyroid hormone,[37] which binds and activates thyroid hormone receptors, resulting in a change in the expression of genes involved in the cell cycle of OPCs and promyelination.[29,38] Although our RNA-seq analysis revealed that OPCs cultured in 3D showed upregulation of genes involved in thyroid hormone transport (*slc16a10*, *slc16a2*, and *crym*), suggesting that OPCs cultured in 3D have more effective uptake of T3 and change the responsiveness to the extracellular differentiation factor, we obtained inconsistent phenotypic results in that the OPCs cultured in 3D showed a low differentiation efficiency compared to those in 2D. In contrast, we detected a reduction in *myrf*,[39] which is key to promoting oligodendrocyte differentiation in OPCs cultured in 3D. Therefore, the differences in differentiation potency from OPCs to oligodendrocytes between the culture dimensions might be due to the changes in the intracellular properties induced by the 3D process as opposed to the changes in the response to extracellular chemical factors, which is supported by previous findings that the extracellular matrix induces epigenetic modification.[40] Although the 3D culture reduced both the proliferation and differentiation of OPCs, the alterations in the expression of genes related to "cellular senescence (GO:0090398)" had different trends depending on genes (data not shown), supporting that OPCs cultured in 3D would not be in the senescence stage.

A 3D culture system using collagen gel allows for ease of modulation of the mechanical properties of the cellular microenvironment by changing the concentration of the collagen solution. In our culture system, we used a similar concentration of collagen to that expected under *in vivo* physiological conditions: about 0.1% of human brain proteins are collagens.[41–43] A low concentration of collagen gel offers changes in the 3D microenvironmental spaces for the encapsulated OPCs as follows: (i) a lower density of collagen fibers, (ii) lower gel stiffness, (iii) a gel network with a larger mesh size, *etc*. We found that OPCs cultured in low-concentration col-

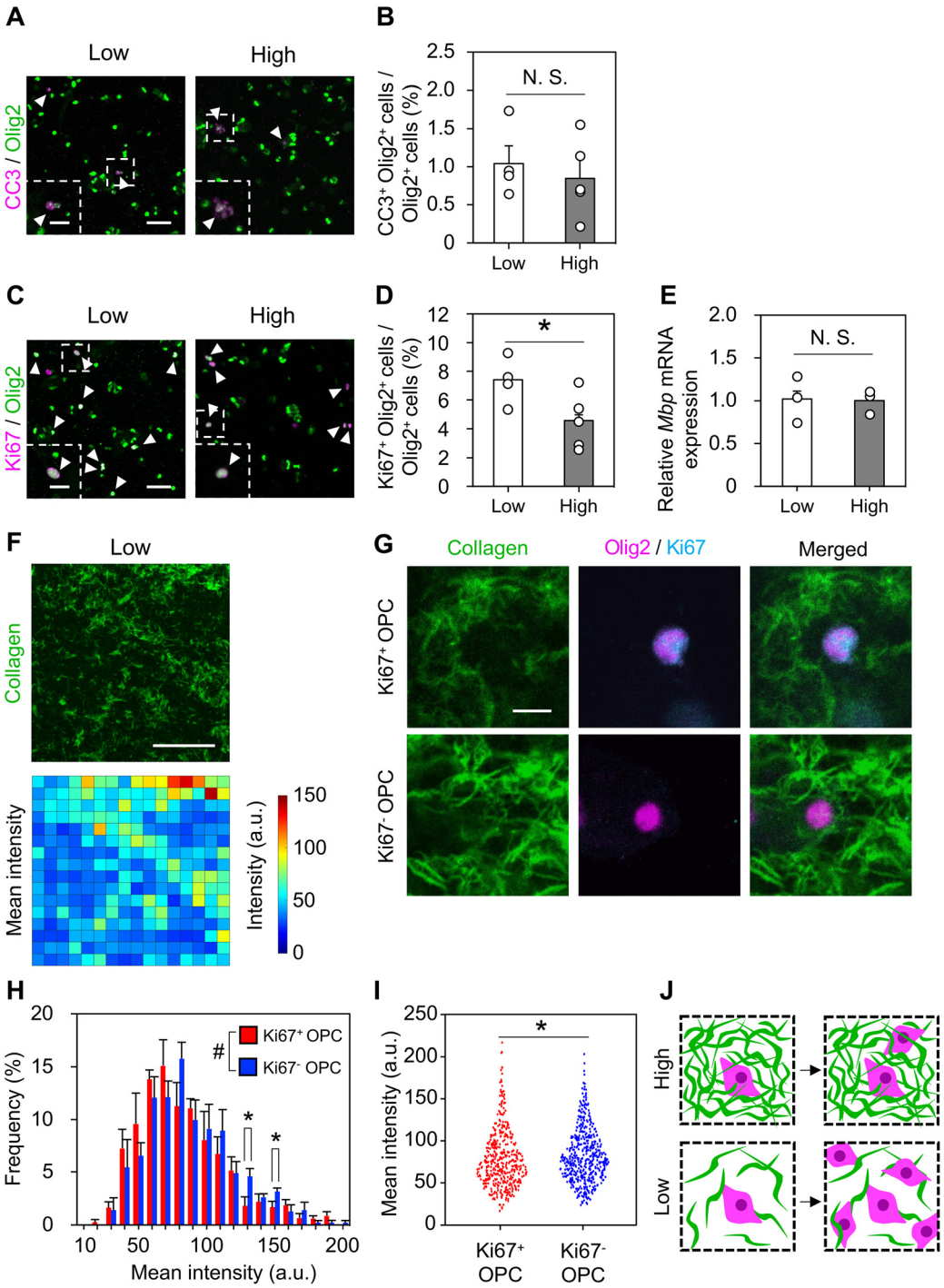

Fig. 4 Collagen concentration modulates OPC proliferation in 3D culture. (A) Representative images of the OPC cultures under the indicated conditions of collagen gel. Cells were stained with CC3 (magenta) and Olig2 (green). The dashed square areas show the high magnification images of CC3 and Olig2 positive cells. (B) Quantification of the percentage of CC3 and Olig2-positive cells (arrowheads in A) in Olig2-positive cells. (C) Representative images of the OPC cultures under the indicated conditions of collagen gel. Cells were stained with Ki67 (magenta) and Olig2 (green). The dashed square areas show the high magnification images of Ki67 and Olig2 positive cells. (D) Quantification of the percentage of Ki67 and Olig2-positive cells (arrowheads in C) in Olig2-positive cells. (E) Quantification of the relative mRNA expression of *mbp* normalized by the internal control (*gapdh*). (F) Representative image of the collagen fibers (upper panel) and the heat map of the fluorescence intensity of collagen fiber (lower panel). (G) Representative images of the OPCs cultured in collagen gel. Cultures were stained with Ki67 (blue), Olig2 (magenta), and collagen I (green). (H) Histograms showing frequency distribution of the mean fluorescence intensity of collagen fiber around the Ki67-positive (red) or negative (blue) OPCs. (I) Strip plots showing the mean fluorescence intensity of collagen fiber around the each Ki67-positive (red) or negative (blue) OPC. (J) Schematic depicting the observation that the collagen concentration regulates OPC proliferation. Error bars represent SEM. $N = 4$ for low and 5 for high in (B and D), $N = 3$ for each in (E), $N = 5$ for each in (H), and $N = 433–507$ cells for (I), $*p < 0.05$ by the Student's t-test and $\#p < 0.05$ by the Kolmogorov–Smirnov test. Scale bars represent 50 μm for low magnification and 20 μm for high magnification.

lagen gel enhanced their proliferation activity compared to those at high concentrations. Since the expression of genes (*nog*, *lrp2*) involved in the "positive regulation of oligodendrocyte progenitor proliferation"[31,32] is suppressed in 3D-cultured OPCs compared to those cultured in 2D, the difference in OPC proliferation between the collagen concentrations might be due to the induction of gene expression that enhances OPC proliferation. We also found that proliferative OPCs were localized around the region of a lower collagen fiber density in the low-concentration collagen gel system (Fig. 4G–I). It is considered that less opportunity for integrin-mediated cell adhesion of OPCs to collagen fibers enhances cellular proliferation activities. However, OPCs on the collagen do not change their proliferation activity,[35] suggesting that the higher proliferation of OPCs in the low-concentration collagen gel would be mainly affected by the lower stiffness and expanded mesh size at low concentrations of collagen gels. A previous study using poly(ethylene glycol)-based hydrogels revealed that the proliferation of OPC lines was dependent on the hydrogel mesh size and stiffness, where the ATP concentration increased more in the hydrogel with a larger mesh size and lower stiffness.[44]

Composite hydrogels such as interpenetrating polymer networks (IPN) should expand the possibilities of precise control of the cell proliferation and differentiation of OPCs. An IPN hydrogel with collagen and hyaluronic acid (HA) as the major components within the ECM of the brain shows an expanded mesh size with thinner filaments within the collagen network, resulting in enhanced neurogenesis compared to the collagen hydrogel.[21] In addition to the stiffness and mesh size of hydrogels, matrix remodelling (*i.e.*, matrix degradability) is also considered as a critical factor in determining cell fate.[33] Indeed, OPCs secrete degradation factors including matrix metalloproteinases,[45] a urokinase plasminogen activator,[46] and hyaluronidase.[47] Future investigation of the cellular and molecular properties of OPCs affected by matrix stiffness and degradability will contribute to establishing a method to evaluate the function of OPCs under specific pathological conditions.

5. Conclusions

We characterized the phenotypic and transcriptomic properties of OPCs under 2D and 3D culture conditions. The 3D culture system used in this study comprised of OPCs embedded in the collagen-type-I ECM. This simple system allowed monitoring of the direct effect of the physical properties of the microenvironment on OPCs, without the influence of other cells in the CNS, such as neurons and glial cells. We found that OPCs cultured in 3D showed reduced proliferation and differentiation into oligodendrocytes compared to those cultured in 2D, which was accompanied by robust changes in the expression of genes involved in OPC proliferation and differentiation. We also found that OPCs cultured in a low-concentration collagen gel enhanced their proliferation activity compared to those cultured in a high-concentration gel. Further investigation of the underlying molecular and mechanical mechanisms of the changes in the OPC response in a distinct ECM might lead to the development of new strategies for demyelinating diseases. Regarding the versatility of this model, using OPCs derived from human embryonic stem cells or induced pluripotent stem cells and tuning the properties of the ECM would become a powerful tool for understanding disease pathology and for drug development of demyelinating diseases.

Author contributions

S. N. performed most of the experiments. A. U. performed the RNA-seq analysis. Y. T. M. and R. M. supervised the study and wrote the manuscript.

Conflicts of interest

The authors declare no competing financial interests.

Acknowledgements

This research was partly supported by MEXT/JSPS KAKENHI (19H03554) and AMED-CREST (22gm1510009). S. N. acknowledges the fellowship from WINGS-QSTEP.

References

1 W. Hu and C. F. Lucchinetti, *Semin. Immunopathol.*, 2009, **31**, 439–453.
2 S. E. Nasrabady, B. Rizvi, J. E. Goldman and A. M. Brickman, *Acta Neuropathol. Commun.*, 2018, **6**, 22.
3 E. Traiffort, S. Morisset-Lopez, M. Moussaed and A. Zahaf, *Int. J. Mol. Sci.*, 2021, **22**, 3426.
4 K. A. Nave and H. B. Werner, *Annu. Rev. Cell Dev. Biol.*, 2014, **30**, 503–533.
5 S. Love, *J. Clin. Pathol.*, 2006, **59**, 1151–1159.
6 M. Cayre, M. Falque, O. Mercier, K. Magalon and P. Durbec, *Front. Cell. Neurosci.*, 2021, **15**, 604865.
7 R. J. M. Franklin and C. Ffrench-Constant, *Nat. Rev. Neurosci.*, 2008, **9**, 839–855.
8 Y. Takanezawa, S. Tanabe, D. Kato, R. Ozeki, M. Komoda, T. Suzuki, H. Baba and R. Muramatsu, *Sci. Rep.*, 2021, **11**, 17825.
9 M. Ito, R. Muramatsu, Y. Kato, B. Sharma, A. Uyeda, S. Tanabe, H. Fujimura, H. Kidoya, N. Takakura, Y. Kawahara, M. Takao, H. Mochizuki, A. Fukamizu and T. Yamashita, *Nat. Aging*, 2021, **1**, 284–294.
10 C. Jensen and Y. Teng, *Front. Mol. Biosci.*, 2020, **7**, 33.
11 A. Jagielska, A. L. Norman, G. Whyte, K. J. Vliet, J. Guck and R. J. Franklin, *Stem Cells Dev.*, 2012, **21**, 2905–2914.

12 A. Jagielska, A. L. Lowe, E. Makhija, L. Wroblewska, J. Guck, R. J. M. Franklin, G. V. Shivashankar and K. J. Van Vliet, *Front. Cell. Neurosci.*, 2017, **11**, 93.
13 T. Lourenço and M. Grãos, *Front. Cell. Neurosci.*, 2016, **10**, 277.
14 S. P. Paşca, *Nature*, 2018, **553**, 437–445.
15 D. Sood, M. Tang-Schomer, D. Pouli, C. Mizzoni, N. Raia, A. Tai, K. Arkun, J. Wu, L. D. Black, B. Scheffler, I. Georgakoudi, D. A. Steindler and D. L. Kaplan, *Nat. Commun.*, 2019, **10**, 4529.
16 H. Tekin, S. Simmons, B. Cummings, L. Gao, X. Adiconis, C. C. Hession, A. Ghoshal, D. Dionne, S. R. Choudhury, V. Yesilyurt, N. E. Sanjana, X. Shi, C. Lu, M. Heidenreich, J. Q. Pan, J. Z. Levin and F. Zhang, *Nat. Biomed. Eng.*, 2018, **2**, 540–554.
17 M. Iwashita, H. Ohta, T. Fujisawa, M. Cho, M. Ikeya, S. Kidoaki and Y. Kosodo, *Sci. Rep.*, 2019, **9**, 3068.
18 N. Egawa, A. Shindo, A. C. Liang, Y. Du, C. Xing, E. K. Lo, K. Itoh, H. Kinoshita, T. Maki, R. Takahashi, R. Sudo, M. Spector, J. Lok and K. Arai, *Stem Cells Dev.*, 2017, **26**, 1078–1085.
19 T. H. Yang, A. R. Thoreson, A. Gingery, D. R. Larson, S. M. Passe, K. N. An, C. Zhao and P. C. Amadio, *J. Orthop. Res.*, 2015, **33**, 668–674.
20 C. P. Addington, J. M. Heffernan, C. S. Millar-Haskell, E. W. Tucker, R. W. Sirianni and S. E. Stabenfeldt, *Biomaterials*, 2015, **72**, 11–19.
21 F. Li, M. Ducker, B. Sun, F. G. Szele and J. T. Czernuszka, *Acta Biomater.*, 2020, **112**, 122–135.
22 M. Hamaguchi, R. Muramatsu, H. Fujimura, H. Mochizuki, H. Kataoka and T. Yamashita, *eLife*, 2019, **8**, e41869.
23 J. Niu, F. Mei, N. Li, H. Wang, X. Li, J. Kong and L. Xiao, *Biochem. Cell Biol.*, 2010, **88**, 611–620.
24 J. Niu, T. Li, C. Yi, N. Huang, A. Koulakoff, C. Weng, C. Li, C. J. Zhao, C. Giaume and L. Xiao, *J. Cell Sci.*, 2016, **129**, 1902–1914.
25 J. Schindelin, I. Arganda-Carreras, E. Frise, V. Kaynig, M. Longair, T. Pietzsch, S. Preibisch, C. Rueden, S. Saalfeld, B. Schmid, J. Y. Tinevez, D. J. White, V. Hartenstein, K. Eliceiri, P. Tomancak and A. Cardona, *Nat. Methods*, 2012, **9**, 676–682.
26 W. Huang da, B. T. Sherman and R. A. Lempicki, *Nucleic Acids Res.*, 2009, **37**, 1–13.
27 W. Huang da, B. T. Sherman and R. A. Lempicki, *Nat. Protoc.*, 2009, **4**, 44–57.
28 J. Janowska, M. Ziemka-Nalecz and J. Sypecka, *Int. J. Mol. Sci.*, 2018, **19**, 331.
29 E. G. Baxi, J. T. Schott, A. N. Fairchild, L. A. Kirby, R. Karani, P. Uapinyoying, C. Pardo-Villamizar, J. R. Rothstein, D. E. Bergles and P. A. Calabresi, *Glia*, 2014, **62**, 1513–1529.
30 R. W. O'Meara, J. P. Michalski and R. Kothary, *J. Signal Transduction*, 2011, **2011**, 354091.
31 T. Kondo and M. C. Raff, *Dev. Biol.*, 2004, **267**, 242–251.
32 M. C. Ortega, O. Cases, P. Merchán, R. Kozyraki, D. Clemente and F. de Castro, *Glia*, 2012, **60**, 851–866.
33 C. M. Madl, B. L. LeSavage, R. E. Dewi, C. B. Dinh, R. S. Stowers, M. Khariton, K. J. Lampe, D. Nguyen, O. Chaudhuri, A. Enejder and S. C. Heilshorn, *Nat. Mater.*, 2017, **16**, 1233–1242.
34 F. Fernández-Klett and J. Priller, *Brain Pathol.*, 2014, **24**, 404–413.
35 C. E. Dorrier, D. Aran, E. A. Haenelt, R. N. Sheehy, K. K. Hoi, L. Pintarić, Y. Chen, C. O. Lizama, K. M. Cautivo, G. A. Weiner, B. Popko, S. P. J. Fancy, T. D. Arnold and R. Daneman, *Nat. Neurosci.*, 2021, **24**, 234–244.
36 Y. L. Huang, C. Y. Liang, D. Ritz, R. Coelho, D. Septiadi, M. Estermann, C. Cumin, N. Rimmer, A. Schötzau, M. Núñez López, A. Fedier, M. Konantz, T. Vlajnic, D. Calabrese, C. Lengerke, L. David, B. Rothen-Rutishauser, F. Jacob and V. Heinzelmann-Schwarz, *eLife*, 2020, **9**, e59442.
37 A. Uyeda, L. Quan, Y. Kato, N. Muramatsu, S. Tanabe, K. Sakai, N. Ichinohe, Y. Kawahara, T. Suzuki and R. Muramatsu, *Glia*, 2021, **69**, 2591–2604.
38 P. Casaccia-Bonnefil and A. Liu, *J. Neurosci. Res.*, 2003, **72**, 1–11.
39 B. Emery, D. Agalliu, J. D. Cahoy, T. A. Watkins, J. C. Dugas, S. B. Mulinyawe, A. Ibrahim, K. L. Ligon, D. H. Rowitch and B. A. Barres, *Cell*, 2009, **138**, 172–185.
40 D. Vigetti, M. Viola, E. Karousou, S. Deleonibus, K. Karamanou, G. De Luca and A. Passi, *FEBS J.*, 2014, **281**, 4980–4992.
41 A. N. Cho, Y. Jin, Y. An, J. Kim, Y. S. Choi, J. S. Lee, W. Y. Choi, D. J. Koo, W. Yu, G. E. Chang, D. Y. Kim, S. H. Jo, S. Y. Kim, Y. G. Kim, J. Y. Kim, N. Choi, E. Cheong, Y. J. Kim, H. S. Je, H. C. Kang and S. W. Cho, *Nat. Commun.*, 2021, **12**, 4730.
42 M. A. Hofman, *Front. Neuroanat.*, 2014, **8**, 15.
43 A. S. Dekaban, *Ann. Neurol.*, 1978, **4**, 345–356.
44 L. N. Russell and K. J. Lampe, *ACS Biomater. Sci. Eng.*, 2017, **3**, 3459–3468.
45 J. H. Seo, N. Miyamoto, K. Hayakawa, L. D. Pham, T. Maki, C. Ayata, K. W. Kim, E. H. Lo and K. Arai, *J. Clin. Invest.*, 2013, **123**, 782–786.
46 M. A. Dent, Y. Sumi, R. J. Morris and P. J. Seeley, *Eur. J. Neurosci.*, 1993, **5**, 633–647.
47 J. A. Sloane, C. Batt, Y. Ma, Z. M. Harris, B. Trapp and T. Vartanian, *Proc. Natl. Acad. Sci. U. S. A.*, 2010, **107**, 11555–11560.